РОЖДЕНИЕ ДВУХ ЗАРЯЖЕННЫХ ПИОНОВ НА ПРОТОНЕ ИЗ ДАННЫХ CLAS/CLAS12

ОЭПВАЯ НИИЯФ МГУ

Е. Л. ИСУПОВ

Jefferson Lab (Newport News, VA, USA)

CLAS12 in Hall B

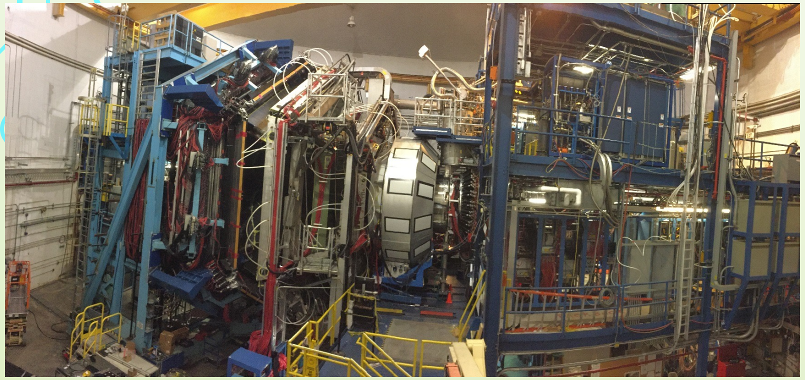

CLAS (1998-2012)

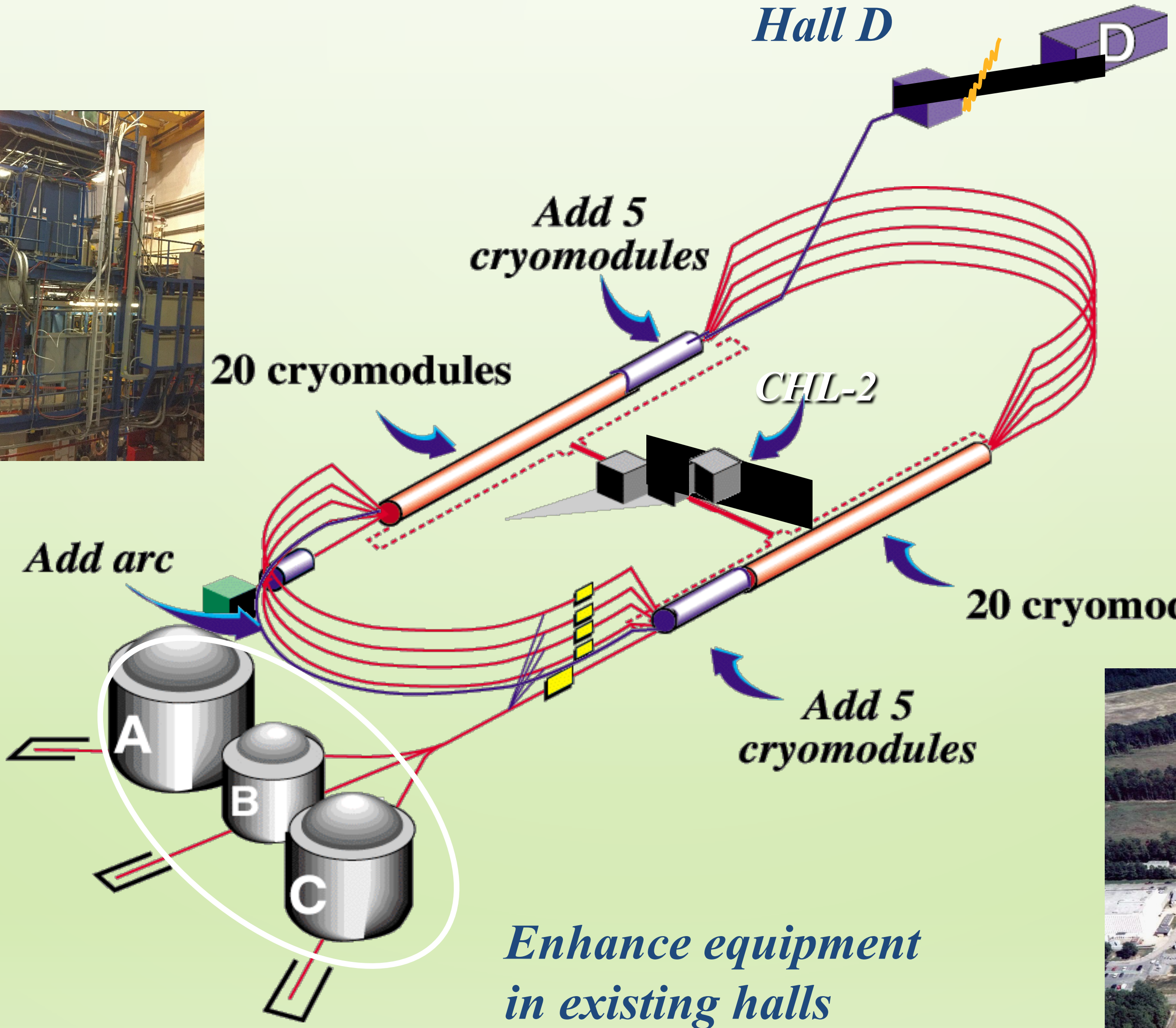

Continuous electron beam with
Energy = 11 GeV
before upgrade: Energy = 6 GeV

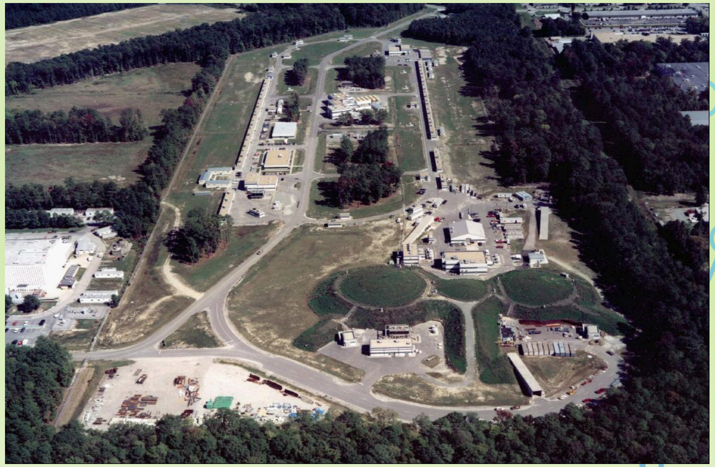

Extraction of $\gamma_v NN^*$ Electrocouplings from Exclusive Meson Electroproduction off Nucleons

Resonant amplitudes **Non-resonant amplitudes**

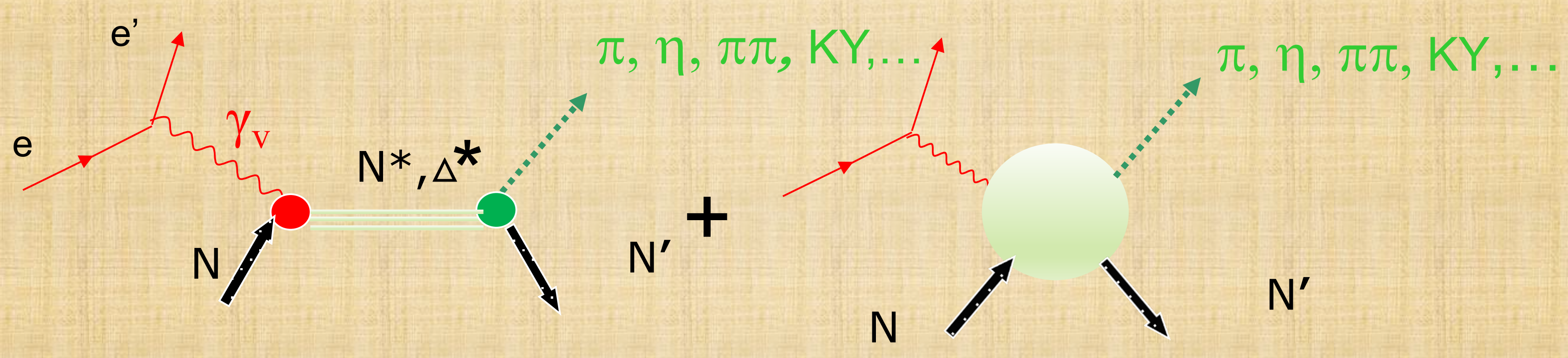

Definition of N* photo-/electrocouplings employed in the CLAS data analyses:

- **Real $A_{1/2}(Q^2)$, $A_{3/2}(Q^2)$, $S_{1/2}(Q^2)$**

I.G. Aznauryan and V.D. Burkert, Prog. Part. Nucl. Phys. 67, 1 (2012)

$$\Gamma_\gamma = \frac{k^2_{\gamma_{N^*}}}{\pi} \frac{2M_N}{(2J_r+1)M_{N^*}} \left[|A_{1/2}|^2 + |A_{3/2}|^2 \right]$$

- **Consistent results on $\gamma_v pN^*$ electrocouplings from different meson electroproduction channels are critical in order to validate reliable extraction of these quantities.**

First results on nucleon resonance electroexcitation amplitudes from $ep \to e'\pi^+\pi^-p'$ cross sections at $W = 1.4$–1.7 GeV and $Q^2 = 2.0$–$5.0\,\mathrm{GeV}^2$

V. I. Mokeev,[1,*] P. Achenbach,[1] V. D. Burkert,[1] D. S. Carman,[1] R. W. Gothe,[2] A. N. Hiller Blin,[3] E. L. Isupov,[4] K. Joo,[5] K. Neupane,[2] and A. Trivedi[2]

[1]*Thomas Jefferson National Accelerator Facility, Newport News, Virginia 23606, USA*
[2]*University of South Carolina, Columbia, South Carolina 29208, USA*
[3]*Institute for Theoretical Physics, Tübingen University, D-72076 Tübingen, Germany*
[4]*Skobeltsyn Institute of Nuclear Physics and Physics Department, Lomonosov Moscow State University, 119234 Moscow, Russia*
[5]*University of Connecticut, Storrs, Connecticut 06269, USA*

(Received 27 June 2023; accepted 31 July 2023; published 25 August 2023)

The electroexcitation amplitudes or $\gamma_v pN^*$ electrocouplings of the $N(1440)1/2^+$, $N(1520)3/2^-$, and $\Delta(1600)3/2^+$ resonances were obtained for the first time from the $ep \to e'\pi^+\pi^-p'$ differential cross sections measured with the CLAS detector at Jefferson Lab within the range of invariant mass $W = 1.4$–1.7 GeV of the final state hadrons, for photon virtualities $Q^2 = 2.0$–$5.0\ \mathrm{GeV}^2$. A good description of the nine independent onefold differential $\gamma_v p \to \pi^+\pi^-p'$ cross sections achieved within the data-driven Jefferson Lab-Moscow State University (JM) meson-baryon reaction model in each bin of (W, Q^2) allows for separation of the resonant and nonresonant contributions. The electrocouplings were determined in the fits of the $\pi^+\pi^-p$ cross sections within three overlapping W intervals with a substantial contribution from each of the three resonances listed above. Consistent results on the electrocouplings extracted from the data in these W intervals provide evidence for their reliable extraction. These studies extend information on the electrocouplings of the $N(1440)1/2^+$ and $N(1520)3/2^-$ available from this channel over a broader range of Q^2. The electrocouplings of the $\Delta(1600)3/2^+$, which decays preferentially into $\pi\pi N$ final states, have been determined for the first time. The reliable extraction of the electrocouplings for these states is also supported by the description of the $\pi^+\pi^-p$ differential cross sections with Q^2-independent masses and total/partial hadronic decay widths into the $\pi\Delta$ and ρp final states.

DOI: 10.1103/PhysRevC.108.025204

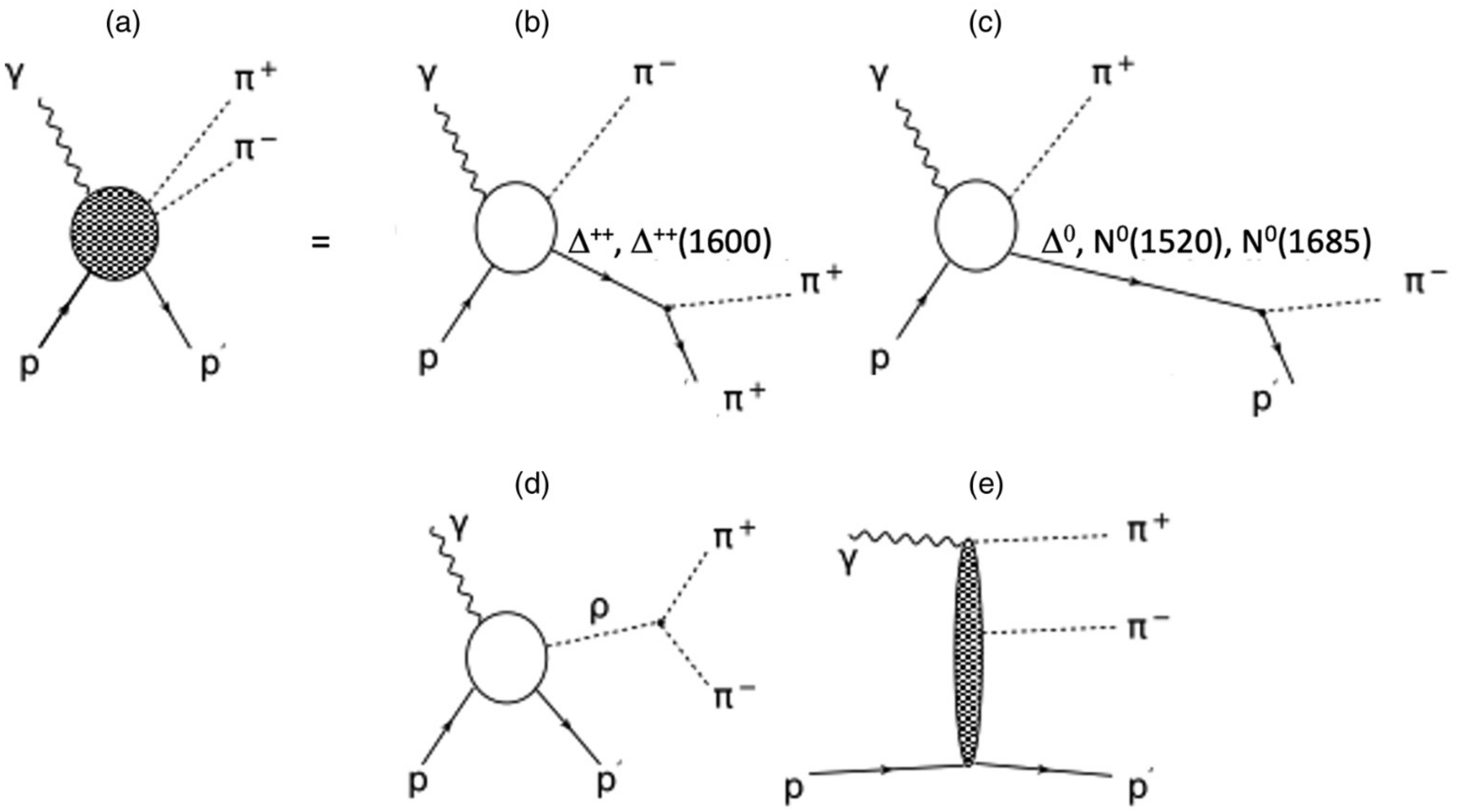

FIG. 2. The $\gamma_v p \rightarrow \pi^+\pi^- p'$ electroproduction mechanisms incorporated at the amplitude level into the JM17 model [11,12,18]: (a) full amplitude; (b) $\pi^-\Delta^{++}$ and $\pi^-\Delta^{++}(1600)3/2^+$ subchannels; (c) $\pi^+\Delta^0$, $\pi^+N^0(1520)3/2^-$, and $\pi^+N^0(1680)5/2^+$ subchannels; (d) ρp subchannel; (e) direct 2π mechanisms.

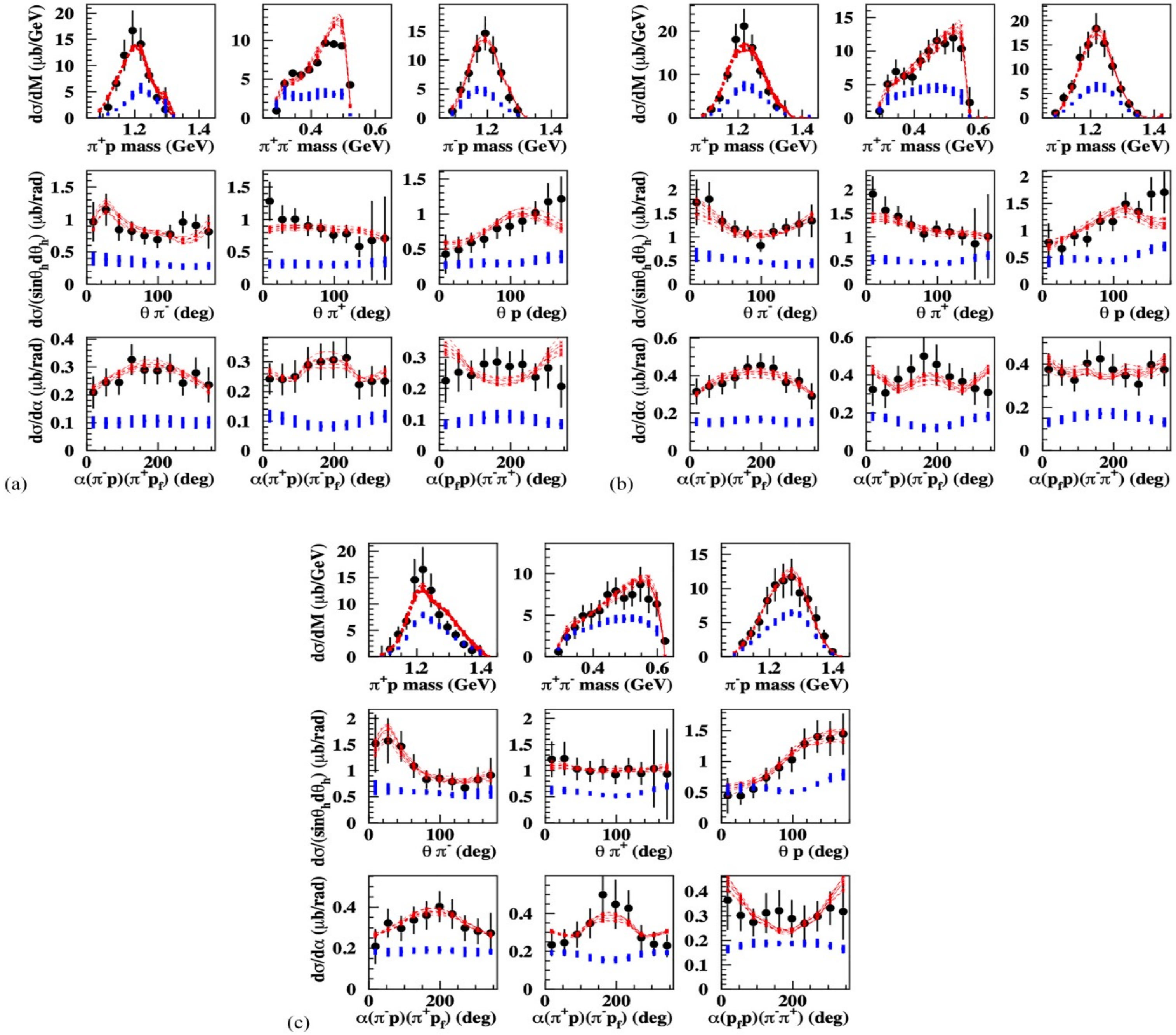

FIG. 7. Fit of the nine onefold differential $\pi^+\pi^-p$ electroproduction cross sections measured with CLAS [47] (in black) achieved within the JM23 model for $W = 1.450$–1.475 GeV (a), 1.500–1.525 GeV, (b) and 1.550–1.575 GeV (c) for $Q^2 = 3.0$–3.5 GeV^2. The data point uncertainties are evaluated as a quadratic sum of statistical and relevant systematic uncertainties. The groups of red curves represent the JM23

Новые Данные по Амплитудам Электровозбуждения Нуклонных Резонансов и Исследования Механизмов Формирования Массы Адронов

- Амплитуды электровозбуждения нуклонных резонансов N(1440)1/2$^+$, N(1520)3/2$^-$ и Δ(1600)3/2$^+$ впервые получены из анализа дифференциальных сечений реакции ep → e$\pi^+\pi^-$p, выполненного в рамках модели JM, развитой в коллаборации НИИЯФ МГУ/Hall B, в диапазоне инвариантных масс конечных адронов W = 1.4–1.7 ГэВ и в интервале модулей квадратов четырехимпульсов виртуальных фотонов Q^2 = 2.0–5.0 ГэВ^2. Хорошее согласие по амплитудам электровозбуждения N(1440)1/2$^+$ и N(1520)3/2$^-$ резонансов из независимого анализа Nπ и $\pi^+\pi^-$p эксклюзивных каналов свидетельствует о надежности результатов. Амплитуды электровозбуждения резонанса Δ(1600)3/2$^+$ были определены впервые.

- Успешное описание амплитуд электровозбуждения резонансов разной структуры Δ(1232)3/2$^+$, N(1440)1/2$^+$, Δ(1600)3/2$^+$ из Лагранжиана КХД достигнутое в методе Дайсона-Швингера с одинаковой зависимостью массы одетого кварка от модуля его четырехимпульса, использованной ранее для описания данных по упругим электромагнитным формфакторам пиона и нуклона, *впервые продемонстрировало возможности доступа к механизмам формирования > 98% массы адронов*.

Phys. Rev. C 108, 025204 (2023)

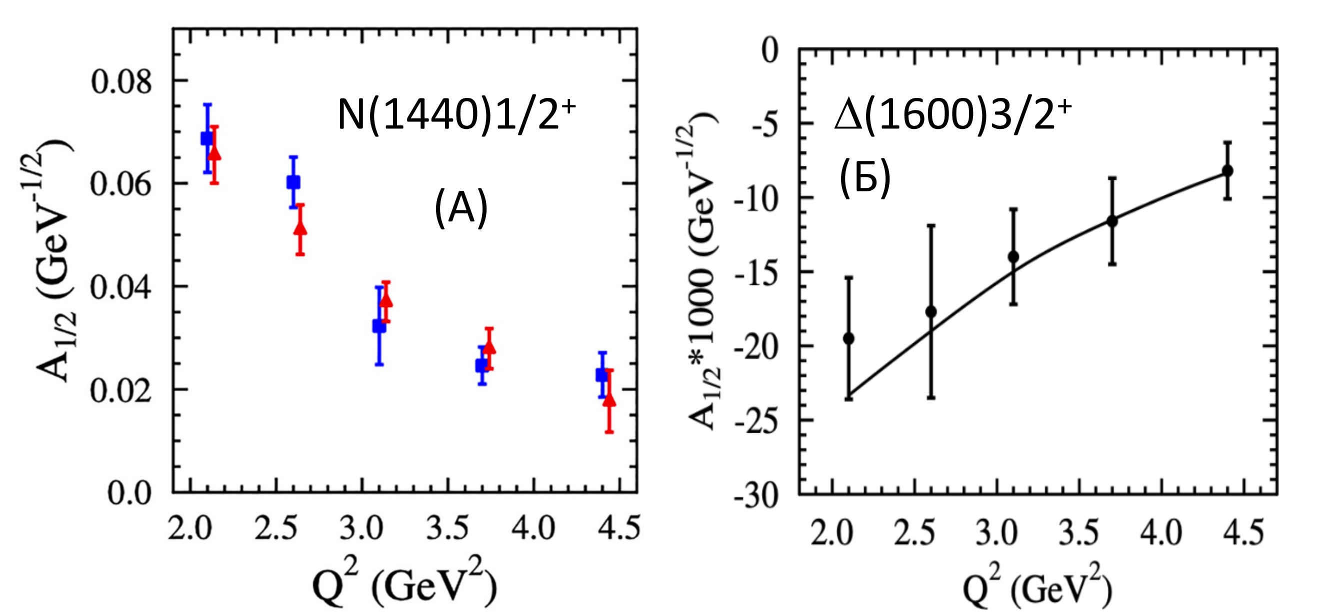

(A) Амплитуда электровозбуждения $A_{1/2}$ резонанса N(1440)1/2$^+$, извлеченная из анализа данных по каналам электророждения Nπ (красные треугольники) и $\pi^+\pi^-$p (синие квадраты).

(Б) Амплитуда электровобуждения $A_{1/2}$ резонанса Δ(1600)3/2$^+$, извлеченная из анализа сечений электророждения $\pi^+\pi^-$p (точки с неопределённостями) и предсказания полученные из Лагранжиана КХД в методе Дайсона-Швингера (черная линия) в 2019 году, когда данные по амплитудам электровозбуждения этого резонанса отсутствовали.

Toward a generative modeling analysis of CLAS exclusive 2π photoproduction

T. Alghamdi,[1,2,*] Y. Alanazi,[3] M. Battaglieri,[4] Ł. Bibrzycki,[5] A. V. Golda,[6] A. N. Hiller Blin,[7] E. L. Isupov,[8] Y. Li,[1] L. Marsicano,[4] W. Melnitchouk,[3,9] V. I. Mokeev,[3] G. Montaña,[3] A. Pilloni,[10,11] N. Sato,[3] A. P. Szczepaniak,[3,12,13] and T. Vittorini[4,14]

[1]*Department of Computer Science, Old Dominion University, Norfolk, Virginia 23529, USA*
[2]*Department of Computer Science, College of Computer Science and Information Technology, Al-Baha University, Al-Baha, Alaqiq 65779, Saudi Arabia*
[3]*Thomas Jefferson National Accelerator Facility, Newport News, Virginia 23606, USA*
[4]*INFN sezione di Genova, I-16146 Genova, Italy*
[5]*AGH University of Krakow, Faculty of Physics and Applied Computer Science, PL-30-059 Kraków, Poland*
[6]*Faculty of Physics, Lomonosov Moscow State University, 119991 Moscow, Russia*
[7]*Institute for Theoretical Physics, Tübingen University, D-72076 Tübingen, Germany*
[8]*Skobeltsyn Institute of Nuclear Physics, Lomonosov Moscow State University, 119234 Moscow, Russia*
[9]*CSSM and CDMPP, Department of Physics, University of Adelaide, 5005 Australia*
[10]*Dipartimento di Scienze Matematiche e Informatiche, Scienze Fisiche e Scienze della Terra, Università degli Studi di Messina, I-98166 Messina, Italy*
[11]*INFN Sezione di Catania, I-95123 Catania, Italy*
[12]*Department of Physics, Indiana University, Bloomington, Indiana 47405, USA*
[13]*Center for Exploration of Energy and Matter, Indiana University, Bloomington, Indiana 47403, USA*
[14]*Università di Genova, I-16146 Genova, Italy*

(Received 21 July 2023; accepted 20 October 2023; published 21 November 2023)

AI-supported algorithms, particularly generative models, have been successfully used in a variety of different contexts. This work employs a generative modeling approach to unfold detector effects specifically tailored for exclusive reactions that involve multiparticle final states. Our study demonstrates the preservation of correlations between kinematic variables in a multidimensional phase space. We perform a full closure test on two-pion photoproduction pseudodata generated with a realistic model in the kinematics of the Jefferson Lab CLAS `g11` experiment. The overlap of different reaction mechanisms leading to the same final state associated with the CLAS detector's nontrivial effects represents an ideal test case for AI-supported analysis. Uncertainty quantification performed via bootstrap provides an estimate of the systematic uncertainty associated with the procedure. The test demonstrates that GANs can reproduce highly correlated multidifferential cross sections even in the presence of detector-induced distortions in the training datasets, and provides a solid basis for applying the framework to real experimental data.

DOI: 10.1103/PhysRevD.108.094030

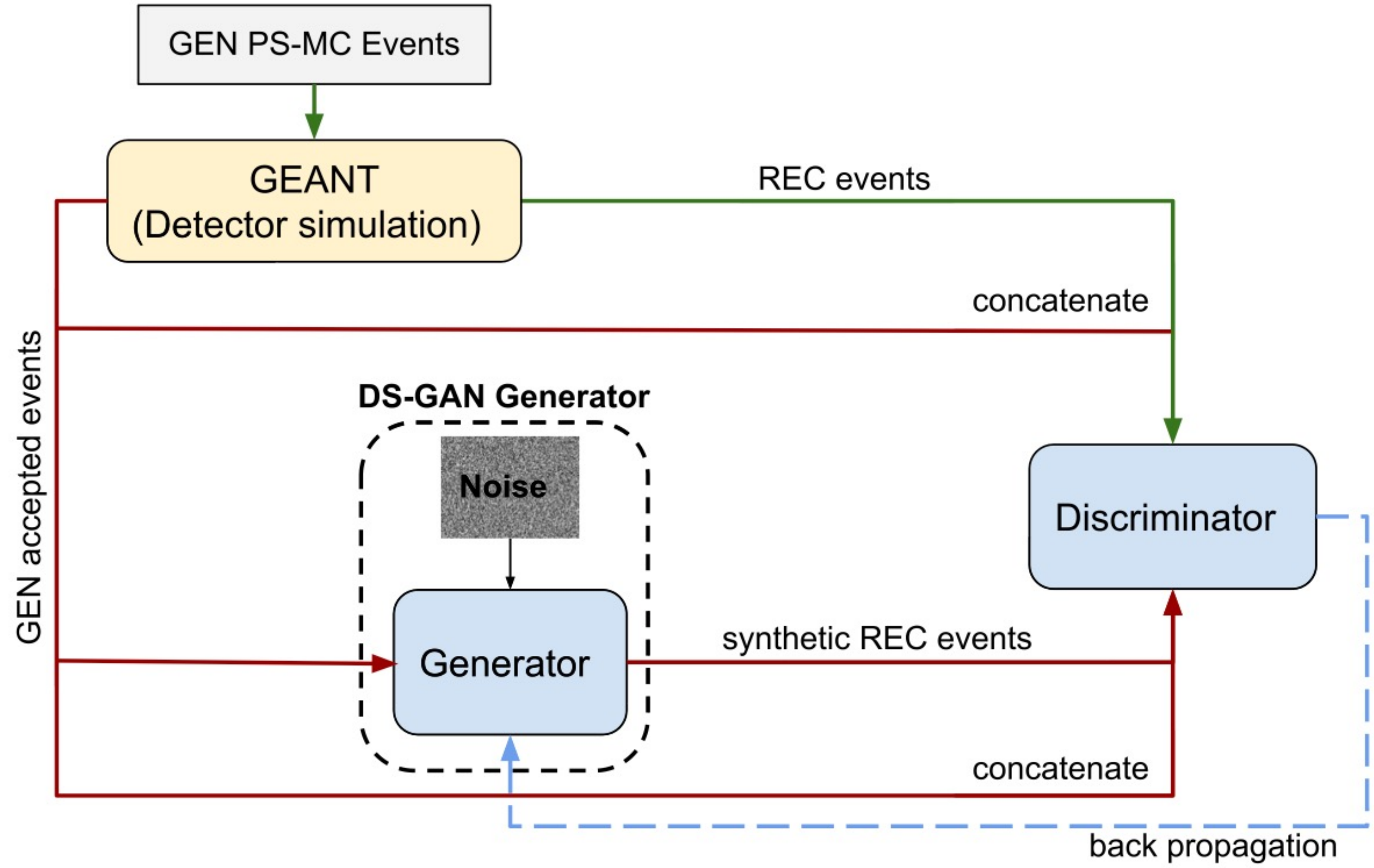

FIG. 9. Schematic view of the ML detector simulation GAN (DS-GAN), where the GAN generator converts input GEN vertex-level events features and noise to REC detector-level events. The training is performed on PS-MC pseudodata passed through the GEANT simulation. Synthetic REC and REC pseudodata are concatenated with GEN PS-MC events and fed to the discriminator.

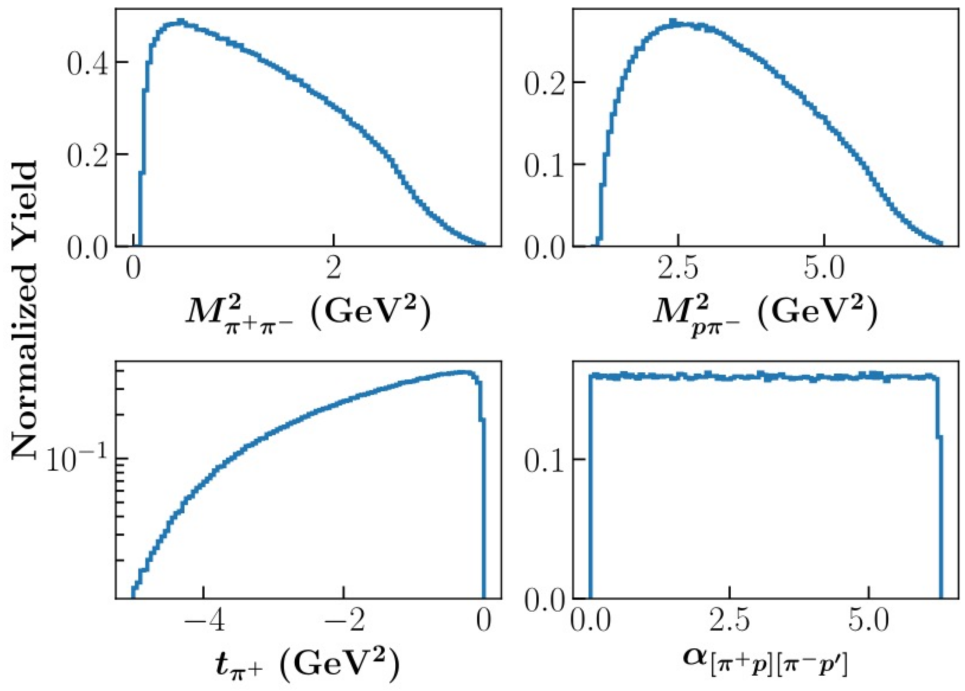

FIG. 2. Normalized 1D projections of events generated with PS-MC: $\pi^+\pi^-$ invariant mass squared (top left), $p\pi^-$ invariant mass squared (top right), square of the four-momentum transferred from the target to the recoil proton, t_{π^+} (bottom left), the angle $\alpha_{[\pi^+p][\pi^-p']}$ in the CM frame between the plane containing the initial target p and π^- three-momenta and the plane formed by π^+ and the scattered proton three-momenta (bottom right).

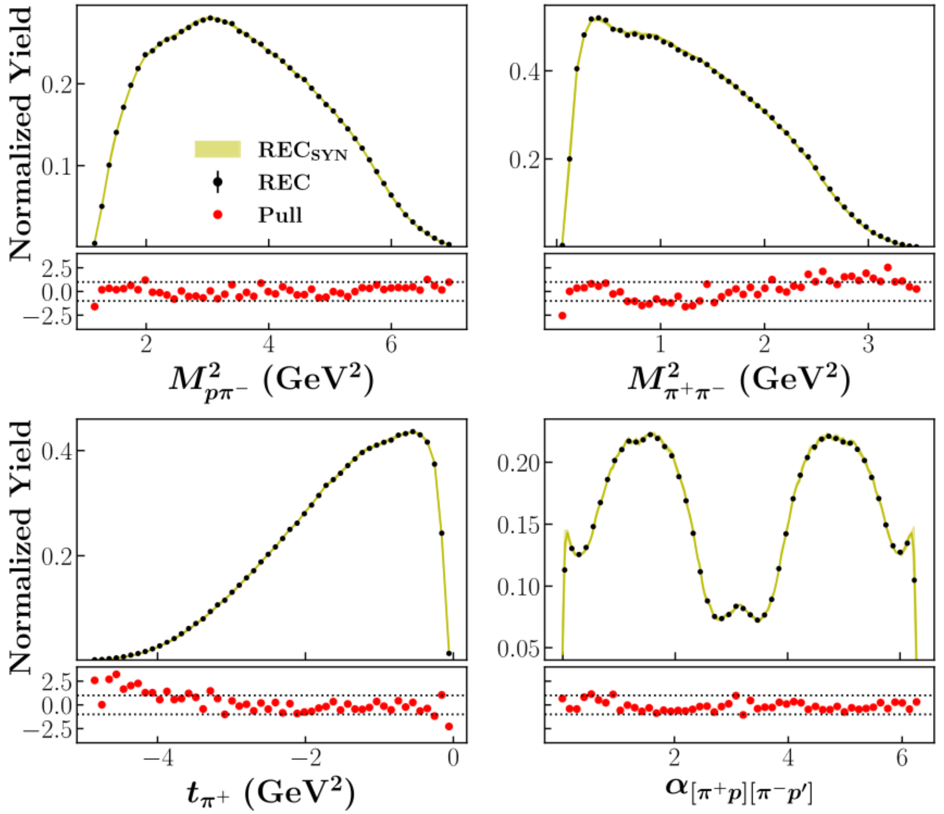

FIG. 11. Training variable PS-MC REC pseudodata distributions (black points) are compared to the synthetic data produced by the DS-GAN (yellow band). The band size reflects the uncertainty estimated using the bootstrap procedure, while the pull distributions (bottom of panels) quantify the agreement between the two, with the horizontal dotted lines corresponding to $\pm 1\sigma$.

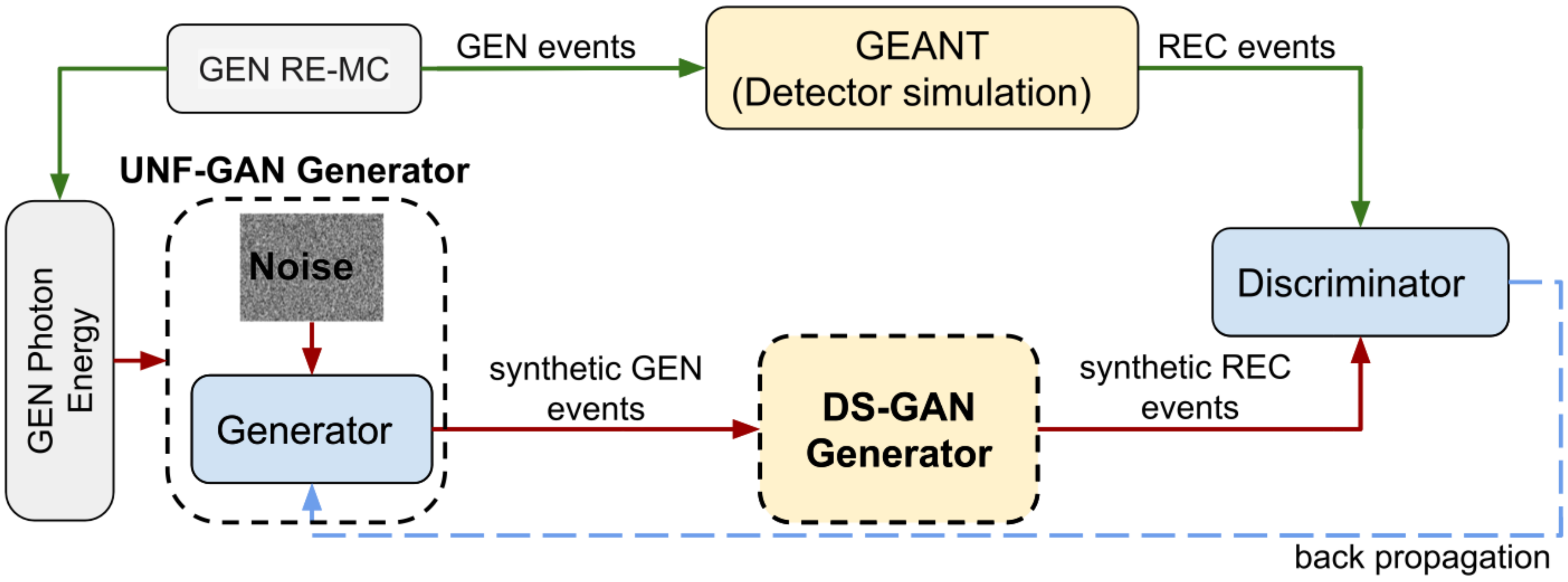

FIG. 10. Schematic view of the UNF-GAN training framework: the UNF-GAN utilizes a generator that converts a GEN photon energy and random noise into synthetic GEN event features, which are passed through the DS-GAN to incorporate detector effect, and are converted into synthetic REC event features. The generator is updated using gradients constructed by a deep neural network discriminator, which compares the features of synthetic and reference REC detector-level events obtained through Geant.

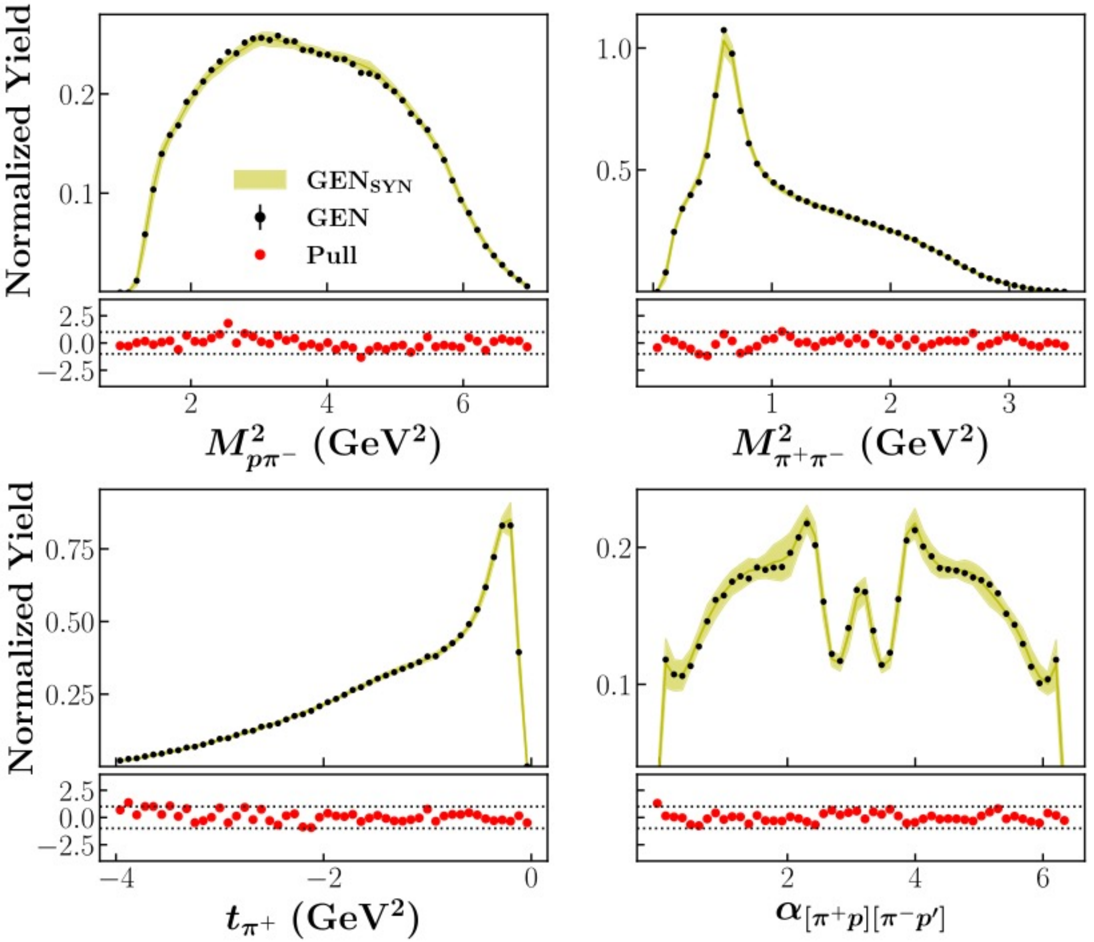

FIG. 15. Comparison of GEN and GEN$_{SYN}$ distributions for the four training variables obtained by the UNF-GAN. Pseudodata were generated using RE-MC.

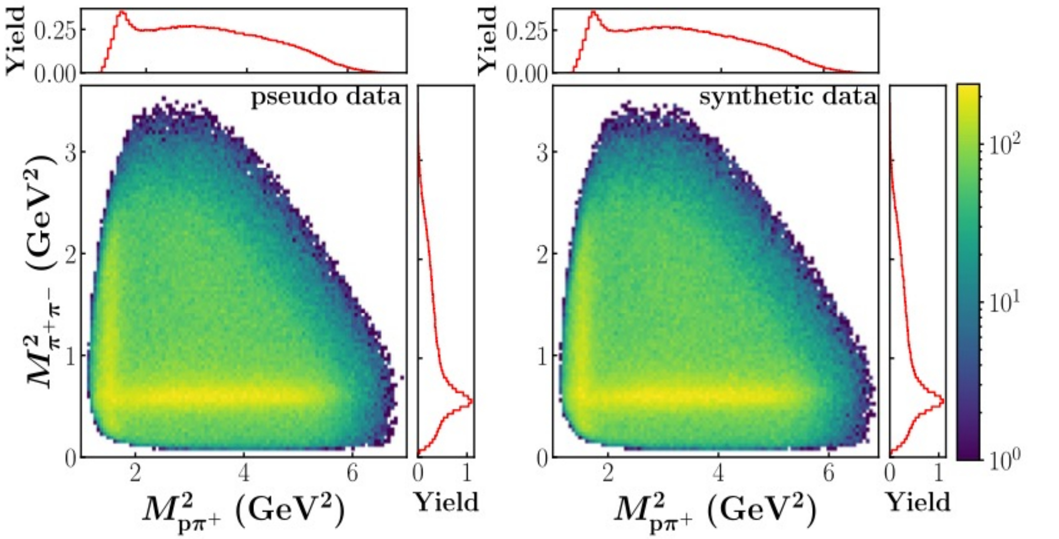

FIG. 16. 2D distributions of $\pi^+\pi^-$ and $p\pi^+$ invariant masses squared in GEN RE-MC pseudodata (left) and synthetic data output of one of the 20 UNF-GANs (right).